J. Geomag. Geoelectr., **49**, 767–789, 1997

Electric and Magnetic Field Galvanic Distortion Decomposition of BC87 Data

Alan D. CHAVE[1] and Alan G. JONES[2]

[1] *Woods Hole Oceanographic Institution, Woods Hole, MA 02543, USA*
[2] *Geological Survey of Canada, 1 Observatory Crescent, Ottawa, Ontario K1A 0Y3, Canada*

(Received April 11, 1995; Revised January 26, 1996; Accepted January 29, 1996)

The BC87 magnetotelluric data exhibit distortions due to three-dimensional structures at all scale sizes, from very local to regional. Previous work has shown that these distortions can sometimes, but not always, be described by an electric field galvanic distortion model, and hence can be removed using a tensor decomposition approach. This work extends the analysis to include galvanic distortion of the magnetic field, and shows its importance for many of the BC87 sites. However, even a combined electric and magnetic field galvanic distortion approach fails for quite a few of the sites studied. This is pervasive for periods shorter than 10 s, suggesting local 3D inductive effects, but model inadequacy at longer periods may indicate a breakdown of the model assumptions, particularly the requirement that the regional electric field be both uniform across the distorting body and comparable to that at the observation point.

1. Introduction

In recent years, it has become apparent that many magnetotelluric (MT) data sets can be described by a background two-dimensional (2D) regional structure coupled with local three-dimensional (3D) non-inductive (usually called galvanic) distortion of the electric and/or magnetic fields. Relevant studies include Chakridi *et al.* (1992), Jones and Dumas (1993), Eisel and Bahr (1993), Jones *et al.* (1993), Kurtz *et al.* (1993), Ogawa *et al.* (1994), Marquis *et al.* (1995), Boerner *et al.* (1995), and Gupta and Jones (1995). Physically, the 3D galvanic distortion is caused by the presence of electric charges along discontinuities or gradients in electrical conductivity associated with small-scale (relative to the background inductive scale length) surface structures. Such charges alter the electric field quasi-statically at all periods, and may also influence the observed magnetic field when the charges deflect regional electric currents. The 3D surface structures cause the observed MT response function elements to be location-dependent mixtures of the 2D regional responses, and distort both their magnitudes and phases.

Quantitative 2D modelling of MT data requires prior identification of regional geoelectric strike and correction of the observed response tensors for galvanic distortion. The most practical approach to date is based on a physical distortion model with decomposition of the MT response into the product of a set of distortion tensors and a 2D regional response tensor. Possibly the most widely applied galvanic distortion tensor parameterization is due to Groom and Bailey (1989), who presented a physical model for galvanic distortion of the electric field which leads to a tensor decomposition written as the product of twist, shear, and anisotropy tensors scaled by a real constant, as described below. The advantage of this parameterization over other approaches is that it isolates the unresolvable shift terms (i.e., the scale factor and anisotropy tensor), and separates the phase effects into resolvable twist and shear tensors. It always exists, since it is derived from a Pauli spin matrix basis which spans a space larger than required for the model (Groom, 1988), and is numerically stable. Other approaches (e.g., Bahr, 1988; Smith, 1995) mix the resolvable and unresolvable terms together, leading to problems in interpretation. Groom and Bailey (1989) further showed that their approach correctly recovers the regional strike and

the two principal regional response functions, except for a static shift on each. Jones and Groom (1993) demonstrated that estimation of the regional strike in the presence of electric field galvanic distortion is inherently unstable, and encouraged the use of some type of tensor decomposition as a routine step in MT data analysis. More recently, Chave and Smith (1994) re-examined the galvanic distortion problem from first principles and derived a set of physical conditions under which a tensor decomposition approach is applicable. They also extended the Groom-Bailey method to include galvanic distortion of the magnetic, as well as the electric field, and demonstrated that magnetic field galvanic distortion can be important to very long periods in some MT data sets.

As the scales of the regional structure and local distorting bodies cover a very wide range, it is not feasible to model galvanic distortion using presently available numerical algorithms. Consequently, it is not possible to use artificial data from numerical models to test electric and magnetic distortion tensor decomposition approaches. As a result, further advances in our understanding of galvanic distortion and its removal must be based on detailed, systematic examination of real data. In this paper, MT data from ten representative locations from the 150 km-long, east-west British Columbia Lithoprobe (BC87) transect (Jones, 1993) are re-analyzed from the raw time series, and then decomposed using both an electric and the full electric and magnetic field distortion model of Chave and Smith (1994). These BC87 responses display complex effects due to both 3D induction and galvanic distortion over scales ranging from that of an electrode array (<50 m) to that of a 150 km by 50 km batholith traversed by the profile (Jones *et al.*, 1993), and hence serve as a challenging test for galvanic distortion decomposition approaches. The results indicate that electric and magnetic field galvanic distortion is present at some, but not all, sites at periods in excess of around 10 s, but that other types of distortion are prevalent at shorter periods that cannot be described using a tensor decomposition approach. For some sites, tensor decomposition fails at all periods, suggesting either (i) large-scale 3D effects, (ii) a breakdown of the conditions under which a tensor decomposition is applicable, or (iii) systematically low error estimates.

2. Galvanic Distortion Tensor Decomposition

The importance of galvanic distortion of both the electric and magnetic fields was apparently first recognized by the Russians. The first English-language papers dealing with the subject (Berdichevsky and Dmitriev, 1976a, b) outlined the problem, but they were not really fully appreciated by the West until much later. Larsen (1977) also briefly stated the electric and magnetic field distortion problem in a theoretical sense, and Larsen (1975) derived a method for removing electric field galvanic effects in the weak distortion limit. An electric-field only tensor approach to galvanic distortion description for a 2D regional Earth was first proposed by Bahr (1984, 1985), and was taken up by Zhang *et al.* (1987), and Groom and Bailey (1989; see also Groom, 1988). These latter two applied a tensor decomposition to the MT impedance tensor which differed from many tensor decompositions proposed in the 1980s in that it is based on a physical model of distortion.

The theory of galvanic distortion tensor decomposition is described by Groom and Bailey (1989), Groom and Bahr (1992), and Chave and Smith (1994). In the latter paper, the form of the decomposition describing distortion of the electric and magnetic fields is derived directly from the integral equation defining their scattering by surface conductivity heterogeneities. If the distortion model is applicable, the relation between the observed 2×2 complex MT response tensor $\mathbf{Z}$ and the purely anti-diagonal scaled regional response tensor $\mathbf{Z_2}$ at a particular frequency is

$$\mathbf{Z} = \mathbf{R} \cdot \mathbf{T} \cdot \mathbf{S} \cdot \mathbf{Z_2} \cdot (\mathbf{I} + \mathbf{D} \cdot \mathbf{Z_2})^{-1} \cdot \mathbf{R}^{\mathbf{T}} \tag{1}$$

where **R** is the rotation matrix which takes the observation coordinate system to the regional one, **T** and **S** are the *twist* and *shear* tensors originally defined by Groom and Bailey (1989), **I** is the identity tensor, and **D** is the magnetic distortion tensor. Chave and Smith (1994) described the indeterminacy associated with tensor decomposition, and showed that the anti-diagonal components of **D** in Eq. (1) are unconstrained by the data. This means that the elements of $\mathbf{Z_2}$ may be scaled by frequency-dependent, complex factors controlled by two real constants, in addition to the usual frequency-independent static shift parameters, without altering the distortion parameters in Eq. (1). All scaling of the true regional 2D impedance $\mathbf{Z_2^t}$, due to both electric static shift factors, called *anisotropy* and *site gain* by Groom and Bailey (1989), and the magnetic static shift factors as discussed in Chave and Smith (1994), have been absorbed into $\mathbf{Z_2}$ in Eq. (1). In the non-inductive limit, and when tensor decomposition is an appropriate description for the distortion, the elements of **T**, **S**, and **D** are real and frequency-independent, but clearly will vary with location. Note that $\mathbf{Z_2}$ is required only to be anti-diagonal, and no further conditions of two-dimensionality are applied, such as requiring phases to lie within prescribed quadrants or imposing causality. In the following, we will present the best-fitting model that we find for the data, and, with the above comment, it must be recognized that this best-fitting model may not necessarily lead to a regional 2D response. Given the error distribution, there may exist other acceptable solutions that yield a 2D regional response but which do not necessarily lead to a minimum misfit. This is commented on further for the decomposition of site 000 below.

By expanding each of the tensor elements in Eq. (1) using a Pauli spin matrix basis and utilizing their algebra, the tensor relation may be written as a set of four simultaneous complex nonlinear equations

$$\zeta_0 = \frac{(e+t)a-(e-t)b+(\varepsilon(1-et)-\gamma(1+et))ab}{1-\gamma\varepsilon ab} \tag{2}$$

$$\zeta_1 = \frac{(1-et)a-(1+et)b+(\varepsilon(e+t)-\gamma(e-t))ab}{1-\gamma\varepsilon ab}\cos 2\theta - \frac{(e+t)a+(e-t)b-(\varepsilon(1-et)+\gamma(1+et))ab}{1-\gamma\varepsilon ab}\sin 2\theta \tag{3}$$

$$\zeta_2 = -\frac{(1-et)a+(1+et)b-(\varepsilon(e+t)+\gamma(e-t))ab}{1-\gamma\varepsilon ab} \tag{4}$$

$$\zeta_3 = -\frac{(e+t)a+(e-t)b-(\varepsilon(1-et)+\gamma(1+et))ab}{1-\gamma\varepsilon ab}\cos 2\theta - \frac{(1-et)a-(1+et)b+(\varepsilon(e+t)-\gamma(e-t))ab}{1-\gamma\varepsilon ab}\sin 2\theta \tag{5}$$

where e and t are the tangents of the shear and twist angles, θ is the regional azimuth (positive clockwise), γ and ε are the diagonal elements of the magnetic distortion tensor, the regional MT response tensor is

$$\mathbf{Z_2} = \begin{bmatrix} 0 & a \\ -b & 0 \end{bmatrix} \tag{6}$$

and the left sides of Eqs. (2)–(5) are combinations of the observed MT response tensor elements with $\zeta_0 = Z_{xx} + Z_{yy}$, $\zeta_1 = Z_{xy} + Z_{yx}$, $\zeta_2 = Z_{yx} - Z_{xy}$, and $\zeta_3 = Z_{xx} - Z_{yy}$.

Inherent symmetries in Eqs. (2)–(5) mean that the equations are invariant to changes in θ by $\pm 90°$ when the sign of e is reversed, a and b are interchanged, and γ and ε are interchanged with a sign reversal. In addition, Smith (1995) noted that the electric field distortion tensors **T** and **S** in Eq. (1) can be re-written in a form appropriate for 2D rather than 3D surface distortion of a 2D regional structure without altering $\mathbf{Z_2}$ or the statistical fit. For electric field-only distortion, Groom and Bailey (1989) showed that the local 2D strike is a function of regional strike and twist

angle. Both of these results mean that ancillary information on the distorting body is required for structural interpretation of the galvanic distortion parameters themselves.

The nonlinear set Eqs. (2)–(5) may be solved numerically using standard methods, either for individual MT sites or, at the penalty of a much larger computational load, simultaneously for a large number of sites under the assumption of a common regional azimuth. They also may be solved frequency-by-frequency or by imposing frequency independence on the distortion parameters at each site.

Chave and Smith (1994) determined the conditions under which a tensor decomposition can be derived from the underlying integral equation which describes the physics of electromagnetic scattering. A tensor decomposition like Eq. (1) is an appropriate description of the distortion only if the background electric field is uniform across the distorting inhomogeneity and can be approximated at the inhomogeneity by its value at the observation point. The first condition, also discussed in Groom and Bahr (1992), is equivalent to requiring that the inductive scale length in the background medium and the source field scale be substantially larger than the maximum dimension of the distorting body. The second condition is more stringent, and depends in a complex way on the background and distorting electrical structures. Note that the cited conditions can be expected to vary considerably with location. For example, the regional field gradient will be much larger very close to a contact in a 2D structure compared to distant points, and the size of distorting inhomogeneities that can be treated, and the frequency range over which they can be modeled using a tensor decomposition, will differ accordingly. Since the physical dimensions of the inhomogeneity are rarely known *a priori*, these conditions cannot normally be applied directly, but their violation may explain some instances where tensor decompositions fail.

The galvanic distortion model implicit in Eq. (1) will not be appropriate in all circumstances, and hence tests for the adequacy of the model must be devised. There are two basic approaches to model assessment: heuristic approaches, and those based on statistics. The former includes *ad hoc* measures of the dimensionality of the regional structure like the phase sensitive skew introduced by Bahr (1988) and used by Eisel and Bahr (1993). Another example is examination of the frequency dependence of the distortion parameters, as advocated by Groom and Bailey (1989) and Chave and Smith (1994). This is based on the premise that the distortion model is realistic when the decomposition parameters are constant over a range of frequencies. For example, it would not be surprising for a local structure to display inductive effects at high frequencies, depending on the actual geometry, conductivity, and nature of the coupling between the surface and regional structures. However, a tensor decomposition might well apply at low frequencies where the anomaly is responding non-inductively. This is most easily tested by first computing the decomposition frequency-by-frequency and then forcing frequency independence over those bands where it seems appropriate, testing the result for statistical goodness-of-fit. Groom and Bailey (1989), Groom and Bahr (1992), Jones and Dumas (1993), and Groom *et al.* (1993) present illustrative examples.

The most widely used statistical goodness-of-fit measure for tensor decompositions is the standard χ^2 test between the observed and modeled response values. The conditions for this test include errors in $\mathbf{Z}$ that are normally distributed, and hence it depends critically on the accuracy of the error estimates for the observed response tensor. Both of these requirements are approximately met, and reliable results achieved, if the data are processed robustly (e.g., Chave and Thomson, 1989) and the errors are computed using the nonparametric jackknife (Thomson and Chave, 1991). The χ^2 test has the advantage that critical values are easily estimated given the equivalent degrees of freedom, and hence standard tests of significance may be utilized. The details depend on the manner in which the tensor decomposition is applied. There are 8 degrees of freedom in the observed MT response tensor at each frequency. For electric field galvanic distortion, there are 7 parameters to be fit if the decomposition is applied frequency-by-frequency, so that the χ^2 test with 1 degree of freedom is appropriate, yielding an expected value for χ^2

of 1 and a 95% level of 3.84. If the decomposition is applied over broad frequency bands, then each frequency has 4 degrees of freedom minus those for the 3 telluric distortion parameters distributed across the band. The expected value of χ^2 is then approximately 4 and the 95% level is about 9.49. However, if the magnetic distortion parameters are included and the decomposition is applied frequency-by-frequency, there are 9 parameters to be fit by 8 data, and the problem is formally underdetermined. Thus, electric and magnetic galvanic distortion decompositions can only be applied over frequency bands. For sufficiently wide bands, and assuming the response estimates are independent, each frequency will have 4 degrees of freedom with a slight reduction due to the 5 distortion parameters which are again assumed to be distributed evenly across the band. This situation can be assessed as for the frequency-independent electric field distortion case.

Groom *et al.* (1993) and Jones *et al.* (1993) use a normalized misfit measure in which the ordinary χ^2 statistic is divided by 4. This can easily be assessed for comparison purposes by dividing the above critical values by 4. However, Groom *et al.* (1993) assert that an acceptable fit is obtained when the normalized misfit is smaller than 4, corresponding to a χ^2 of 16. This is approximately the 95% value for 8 degrees-of-freedom, and does not correctly account for the reduction in degrees-of-freedom when parameters are being fit to the data. As noted above, the proper 95% χ^2 value for frequency-independent parameters is 9.49, not 16, so a normalized misfit should be smaller than 2.5 rather than 4. It is recommended that the correct misfit criterion be adopted, suitably normalized when necessary. However, a single misfit statistic can be an inadequate description of how well the model fits the data; Groom *et al.* (1993) strongly advocate inspection of the fit of the model parameters to the data to ensure that significant features in them are being described.

Finally, for the tensor decomposition Eq. (1) to be useful, it is essential not only to correct the response function estimates themselves, but also to derive meaningful confidence limits on the resulting regional responses. This is not a simple matter when the transformation is nonlinear, as in Eqs. (2)–(5). Parametric approaches are hopeless because the distributions of the elements of Eq. (1) are unknown, and probably not analytically derivable. The bootstrap-like approach of Groom *et al.* (1993), using realizations generated from the mean values of the estimates and their variances under a Gaussian distribution assumption, is one nonparametric solution, but may fail if normality is violated. The jackknife makes no distributional assumptions whatsoever, and is easily implemented, being based on successive resampling with replacement of the available data. However, use of the jackknife does require that the raw time series, or at least spectra, are available. Chave and Smith (1994) describe the implementation of the jackknife for tensor decompositions using delete-one estimates of the observed MT response tensor as will be applied in this paper.

3. The BC87 Data

As a component of the Lithoprobe Southern Cordilleran project, twenty-seven wideband MT sites were collected along a 150 km long reflection seismic line in southeastern British Columbia in 1987. The tectonic setting of the resulting BC87 transect is described by Jones (1993). Figure 1 shows a simplified geological map of the region together with the ten BC87 MT sites selected for the present study. These ten stations were chosen to span the different geological provinces, and hence presumably represent the range of distorting structures. All the sites were either 7-channel remote-referenced, or collected as ten channel (2 times 2 electric, plus 3 magnetic) pairs in close proximity (typically 1 km apart).

At the west end of the transect, sites 901/902 are a closely spaced ten channel pair situated on the Valhalla gneiss complex, a Cretaceous to early Tertiary metamorphic core complex, and approximately 15 km west of the Slocan Lake Fault, a crustal-scale Eocene normal fault. Site 000

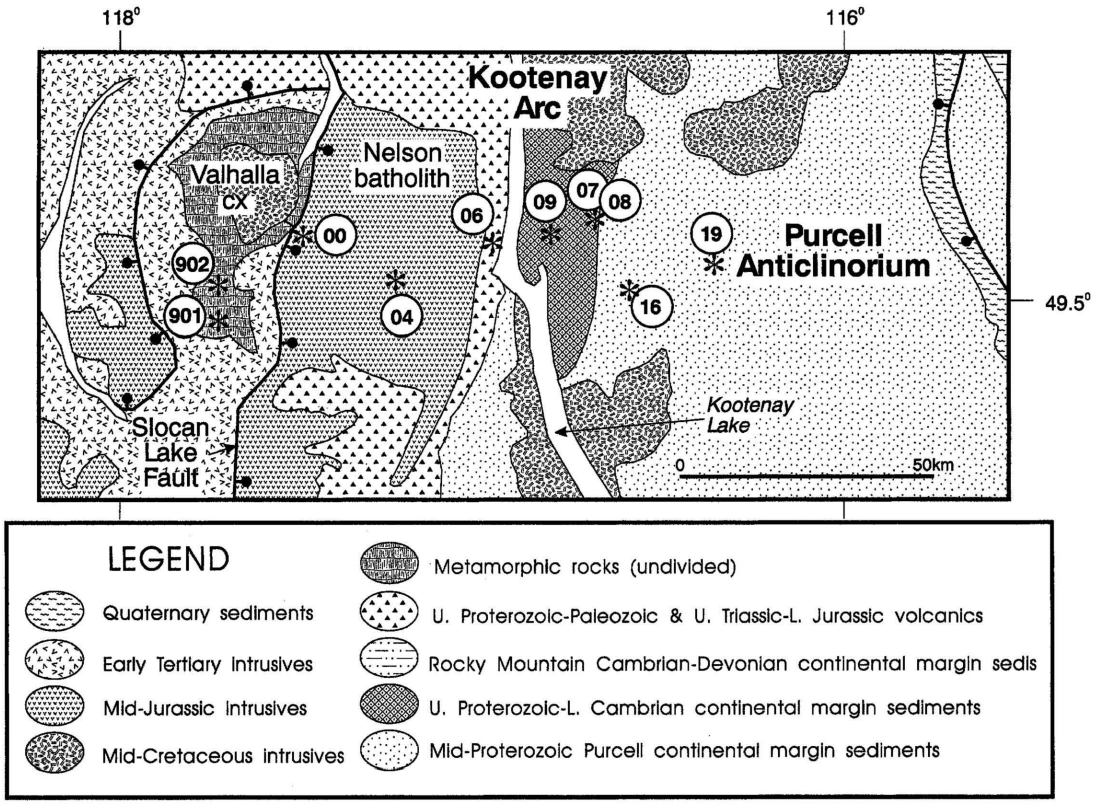

Fig. 1. Simplified geologic map of the BC87 region showing the locations of the MT sites used in this study (numbers in circles). Overlapping circles indicate local/remote 10-channel pairs. The patterns in the bottom panel define the surface geology, while the major geological features are defined in the top panel.

is located in the Slocan Valley on the surface expression of the Slocan Lake Fault and immediately to the east of the Nelson batholith, a mid-Jurassic intrusion into the accreted terranes west of the Kootenay Arc. Site 004 is located close to the centre of the Nelson batholith. Site 006 is located just off and to the east of the batholith. Sites 009 and 007 are located on upper Proterozoic to lower Cambrian continental margin sediments associated with the Kootenay Arc. Site 008 is immediately to the east of 007 (for which it constitutes half of a ten channel pair) and on the mid-Proterozoic Purcell continental margin sediments. Sites 016 and 019 are further to the east on the Purcell Anticlinorium. (For a geological description of the Purcell Anticlinorium, and an analysis and interpretation of over 200 MT sites recorded on it, see Gupta and Jones, 1995.)

The major features of the BC87 dataset are described by Jones *et al.* (1988). In particular, those authors stress the presence of large scale 3D distortion at many of the sites, as evident by out-of-quadrant phases for the TM mode near and on the Nelson batholith, and pervasive small scale distortion. Distortion effects and their removal from some of the data can be found in Groom and Bahr (1992) (sites 000, 017, and 902), Groom *et al.* (1993) (sites 902 and 000), and Jones and Groom (1993) (sites 007 and 008). Jones *et al.* (1993) give a more comprehensive analysis of the distortion in the BC87 data and its removal by decomposition.

4. Comparison of Phoenix and Robust Estimates

For each of the ten sites, the raw time series recorded at a 12 Hz rate (Phoenix "low-range" continuous data) were re-processed using an extension of the robust remote reference method of Chave and Thomson (1989), yielding the tensor MT response over the range 0.667–1820 s. The BC87 data sampled at higher rates were not used. The major improvements to the Chave and Thomson approach include automatic use of variable section sizes such that the frequency of interest is always of order the inverse section length, complete implementation of nonparametric jackknife error estimates (Thomson and Chave, 1991), and a new method for automatically controlling leverage by anomalous magnetic field values in addition to robust removal of outliers in the electric field. The use of short data sections has empirically been shown to facilitate detection of electric field outliers, especially the most common form which occurs in correlated clumps rather than as a rare isolated anomalous point. Leverage control based on the size of the hat matrix diagonal elements has been described by Chave and Thomson (1992) and will be elaborated on elsewhere. Leveraging is quite significant in the BC87 data, especially at the shortest periods. For each of the time series, the MT responses were computed at exactly the same frequencies used in the original Phoenix Geophysics processing to simplify application of the system response corrections, and the delete-one values were saved for later application to tensor decomposition as described earlier.

Phoenix processing of these "low-range" data consisted of real-time cascade decimation using the Wight and Bostick (1980) scheme coupled with weighted averaging of the spectral estimates from the various substacks of the data; this is similar to method 4 described by Jones *et al.* (1989). The weight on each substack of eight spectral estimates was based on a parametric estimate of the variances of the two off-diagonal elements of the MT impedance tensor (Z_{xy} and Z_{yx}) with rejection of substacks whose weight fell below a threshold value.

Despite the different approaches to MT response estimation, the Phoenix and robust remote reference controlled leverage MT tensor estimates generally compare quite favourably in the mid-band (5–500 s). At longer periods, the robust results are generally smoother and more consistent from frequency-to-frequency, whereas at shorter periods, the Phoenix results appear superior. The former is due to better control of leverage and outlier effects by the robust controlled leverage algorithm. The Phoenix processing utilizes thresholding to discard noisy data segments, and hence its better performance at short periods might be due to the absence of data with low signal-to-noise ratio near the MT "dead band" around 1 s. When such noisy segments are pervasive, a robust program might, in fact, discard the infrequent good (i.e., high SNR) segments rather than the bad ones. To test this hypothesis, coherence thresholding using the multiple coherence between the electric and two horizontal magnetic channels was implemented as a preliminary stage in robust controlled leverage processing. This had no effect except to widen the error bars as the coherence threshold and hence the number of discarded sections rose. It is possible that use of the partial, rather than multiple, coherence would yield a better result, especially if there is a polarization bias associated with low SNR data segments that is obscured by multiple coherence thresholding, but further work is required to ascertain this.

However, there is a substantial discrepancy between the error estimates from the Phoenix parametric approach and the nonparametric jackknife results from the robust algorithm. Thomson and Chave (1991) demonstrated the reliability and accuracy of the jackknife approach through simulation over a variety of error distributions, as well as the concomitant unreliability of parametric approaches. Better consistency of the jackknife, as compared to the parametric errors, is demonstrated in Fig. 2, which compares the Phoenix and robust controlled leverage estimates for Z_{xx} and Z_{xy} at site 902 in normalized (Studentized) form. In the upper panel, the difference between the two estimates normalized by the jackknife standard error is shown, while at the bottom, the same quantity is normalized by the parametric standard error from the Phoenix processing.

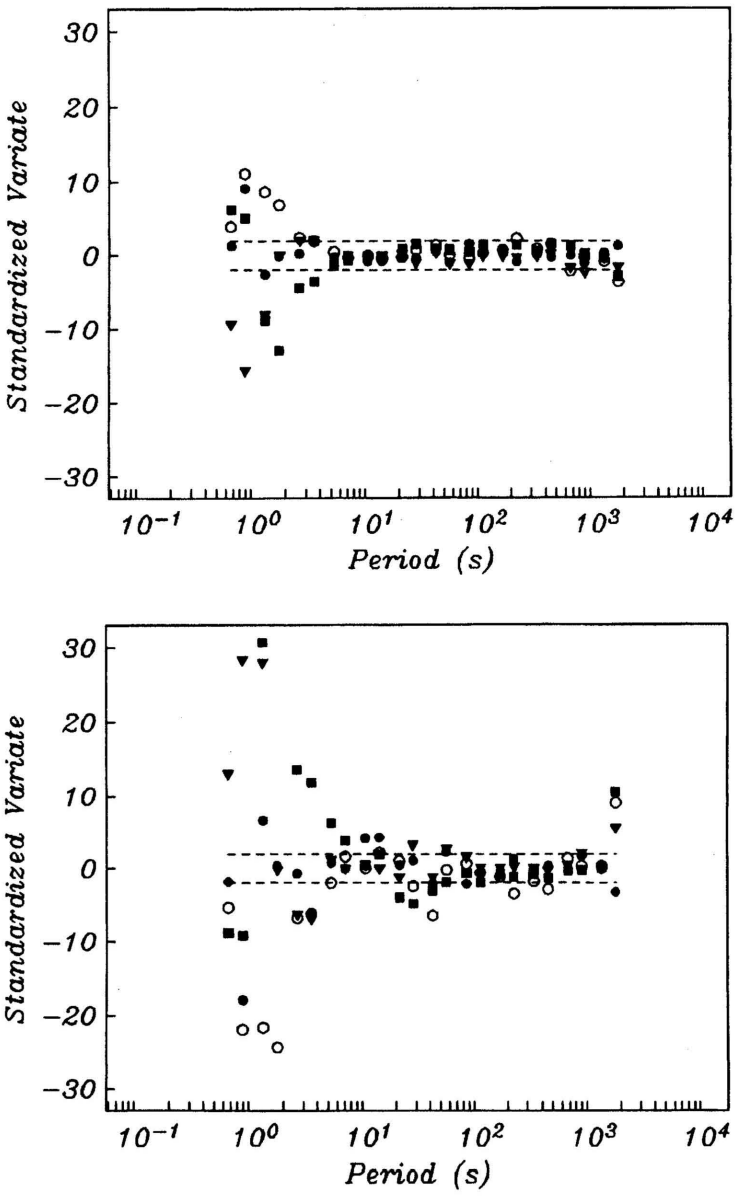

Fig. 2. The normalized (Studentized) residual $(x1-x2)/s$ where $x1$ and $x2$ are the robust controlled leverage and Phoenix estimates of Z_{xx} and Z_{xy} and s is the jackknife estimate of the standard error (top panel), and $x1$ and $x2$ are the Phoenix and robust controlled leverage estimates of Z_{xx} and Z_{xy} and s is the Phoenix parametric estimate of the standard error (bottom panel) plotted against period. The symbols denote the real and imaginary parts of Z_{xx} (open and closed circles) and Z_{xy} (solid squares and triangles), respectively. The horizontal dashed lines show the 2 standard error bounds inside which 95% of the estimates should lie for a Gaussian model. The ordinate is in units of s due to the standardization.

In the first instance, the normalized difference lies within two standard errors of the origin at most periods over 5 s, demonstrating consistency of the estimates with both each other and the jackknife standard error. At periods under 5 s, the estimates diverge from the expected range by a substantial margin, suggesting either that the jackknife standard error is too small or that one

of the estimators is biased; the latter is suggested by comparison of the MT response estimates themselves. This bias is quite large, amounting to up to 20 standard errors in one instance. In contrast, for the lower panel, both estimates are somewhat consistent with the standard error between 10 and 1000 s, although there is more variation than for the jackknife standard error and also more than would be expected for a Gaussian model. There is a large discrepancy at the longest and at short periods, with frequent deviation exceeding 10 and peak values of 30 standard errors. These results strongly suggest that the Phoenix standard errors are inaccurate. The example in Fig. 2 is typical and not extreme. Direct comparison of the parametric and jackknife standard errors indicates that the former are usually, but not always, too large by a factor of 2–5 over the periods studied, and further suggest that the parametric error estimates are too erratic to be considered reliable.

5. Decomposition of BC87 Data

5.1 Valhalla gneiss complex response (901/902)

Stations 901/902 are situated on the Valhalla gneiss complex and in close proximity, as they are a ten channel pair. Their MT response tensors and decomposition parameters are virtually identical, and hence only the decomposition of site 902 will be described. Jones *et al.* (1993) have presented a standard 2D analysis of these data, and showed that a 2D model neither fits the data nor yields a physically-interpretable response.

Figure 3 shows the χ^2 misfit and electric field distortion parameters for a frequency-by-frequency electric field distortion tensor decomposition. The twist is approximately frequency-independent over 1–100 s, but changes abruptly at longer periods. However, the shear and azimuth are both frequency dependent over most of the range. The χ^2 misfit is not acceptable at any period, and increases sharply as period drops, suggesting that magnetic distortion might be present. The distortion parameters are similar to those shown in Fig. 3a of Jones *et al.* (1993), except for a change in azimuth by 90° and a reversal in sign of the shear (under which Eqs. (2)–(5) are invariant with a suitable interchange of the principal responses, as noted earlier).

Figure 4 shows the χ^2 misfit and electric field distortion parameters for an electric and magnetic field distortion tensor decomposition applied over 3-frequency-wide running average bands. The χ^2 misfit is acceptable at periods longer than 5 s, but the distortion parameters are markedly period dependent and very similar to those in Fig. 3. This is especially true of the azimuth; the shear is somewhat less period dependent below 100 s. The magnetic field distortion parameters display a similar variation with period. The variability of the parameters can be smoothed by increasing the width of the running average bands at the cost of an unacceptable misfit; the distortion parameters continue to be strongly period dependent.

By statistical criteria, attempts to fit frequency-independent electric and magnetic field distortion models over the whole frequency range to this site consistently fail, typically displaying χ^2 misfits of at least 100 at all periods. However, comparison of the electric field decomposition parameterization compared to the response functions shows that most of the data are fit well over much of the band (Fig. 5); the fit is worse at short (due to magnetic field distortion effects) and long periods. The misfit is also worse in the diagonal, as compared to the anti-diagonal, parts of the MT response tensor, as was also shown in Jones *et al.* (1993).

Neither of the Valhalla gneiss complex sites can be completely explained by 3D galvanic distortion of a 2D structure. A χ^2 misfit level of 100 infers that the data are being fit to a level of about four times the standard errors, which are typically a degree in phase and 2.5% in apparent resistivity—so that the data are being fit at the 4–5 degree level. Both the frequency-dependence of the distortion parameters and the inability of an electric and magnetic distortion model to change the nature of the fit suggest 3D inductive effects, perhaps reflecting the complexity of the regional geology (Fig. 1). Alternately, the poor fit may reflect a breakdown of the tensor

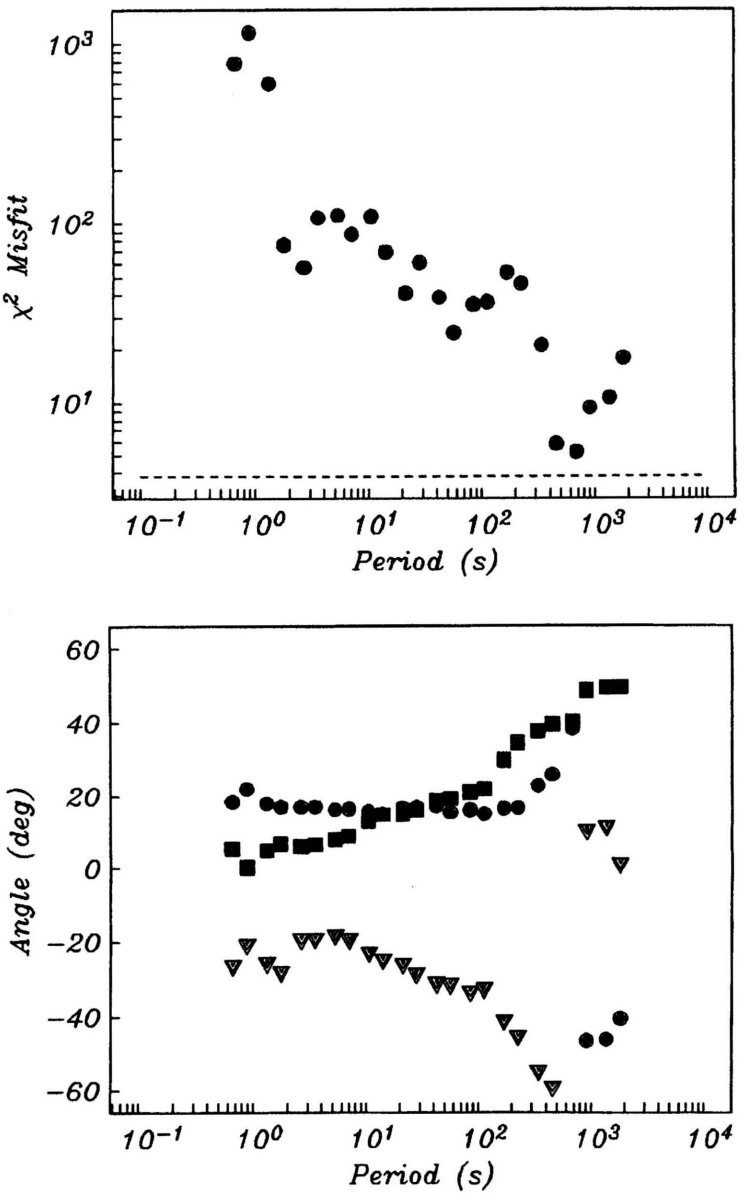

Fig. 3. The χ^2 misfit (top panel) and electric field distortion parameters (bottom panel) plotted against period for a frequency-by-frequency electric field galvanic distortion decomposition of the MT response at site 902. The dashed horizontal line in the top panel denotes the 95% critical value for 1 degree of freedom. The three quantities shown in the bottom panel are twist (circles), shear (squares), and regional azimuth (triangles).

decomposition model when the regional electric field at the observation point is not similar to, or uniform across, the distorting body.

5.2 Nelson batholith response (Sites 000 and 004)

Site 000 is located on the western border of the Nelson batholith, whereas site 004 is close to its center (Fig. 1). While their raw MT responses are dissimilar, the distortion decomposition

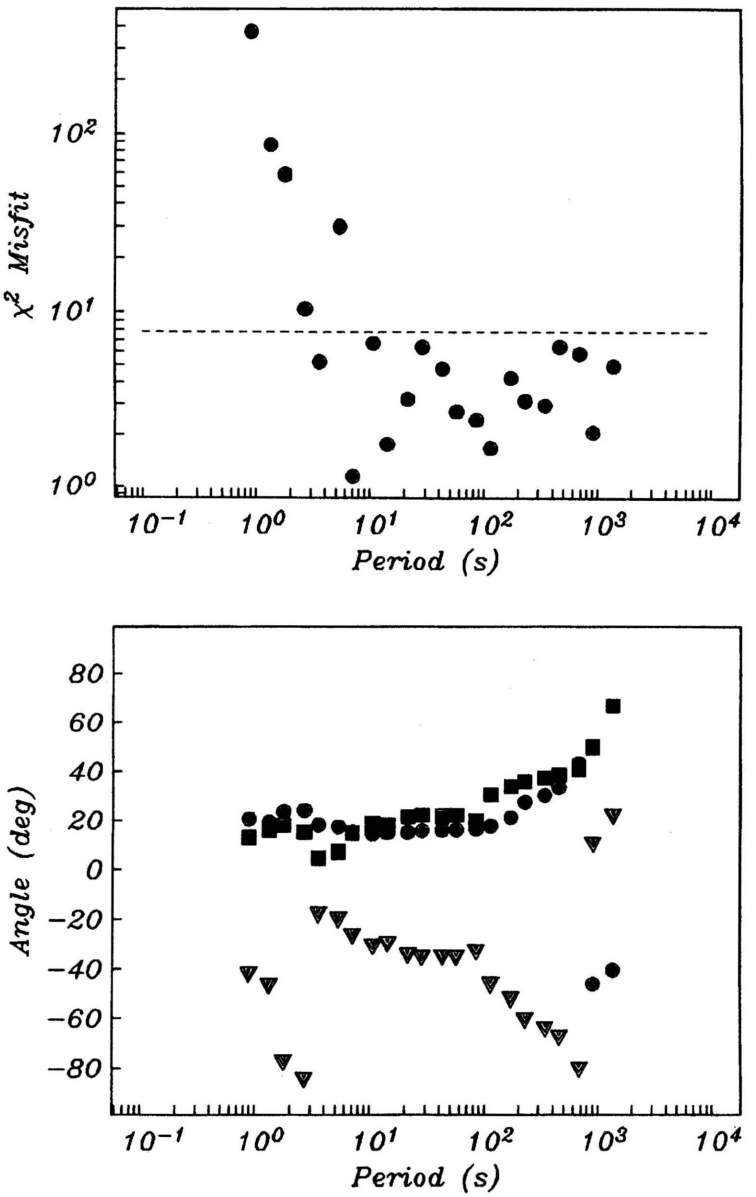

Fig. 4. The χ^2 misfit (top panel) and electric field distortion parameters (bottom panel) plotted against period for an electric and magnetic field galvanic distortion decomposition of the MT response at site 902 computed over running average bands 3 frequencies wide. The dashed horizontal line in the top panel denotes the 95% critical value for 3 degrees of freedom. The three quantities shown in the bottom panel are twist (circles), shear (squares), and regional azimuth (triangles).

parameters are quite alike, and hence they will be described together. Figure 6 shows the χ^2 misfit and electric distortion parameters for a frequency-by-frequency fit of an electric field only tensor decomposition at site 000. The shear is nearly period independent over the entire range, displaying some scatter at the longest periods. However, both the twist and the azimuth vary substantially with period. The χ^2 misfit is only acceptable at periods longer than about 40 s,

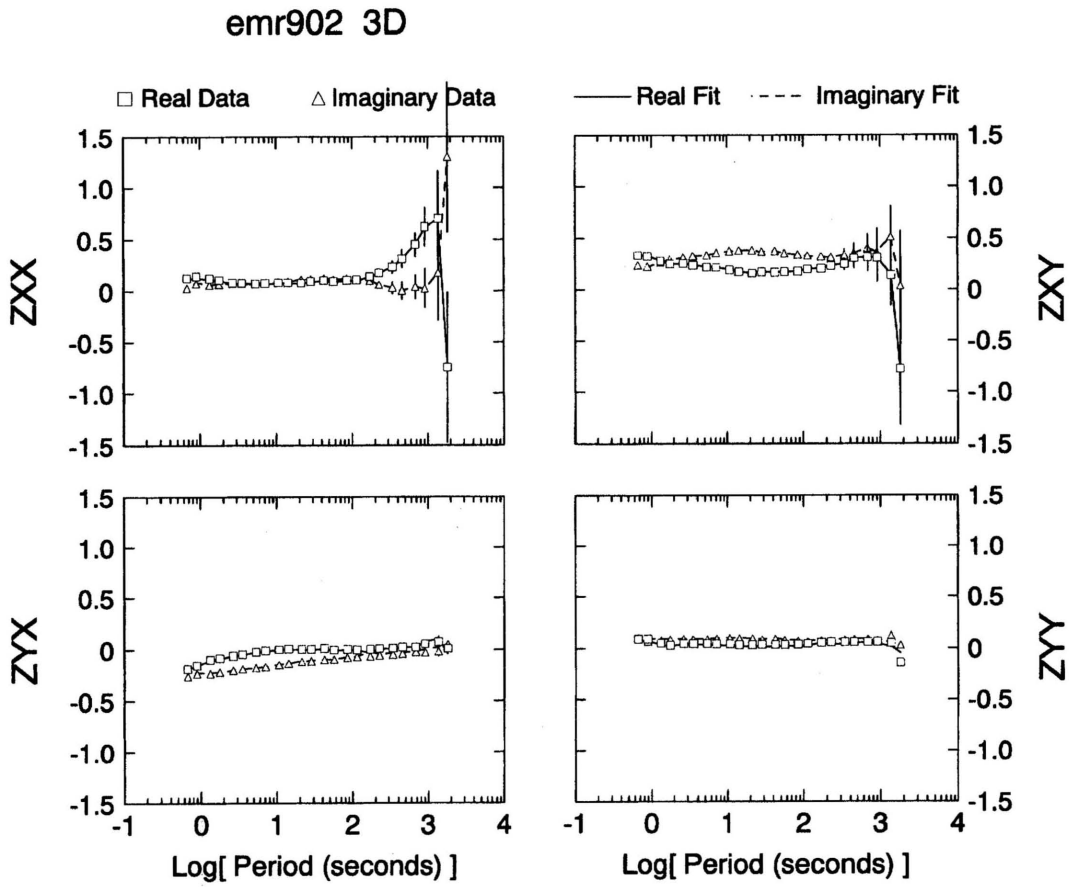

Fig. 5. The fit of the frequency-independent electric field only decomposition model to the data from site 902. The response functions are shown as symbols with 95% error bars, with squares and triangles denoting the real and imaginary parts, respectively. The model responses are shown as solid and dashed lines for the real and imaginary parts, respectively.

and rises with decreasing period below that point.

Figure 7 shows the χ^2 misfit and electric distortion parameters for an electric and magnetic distortion model fit over 3-frequency-wide running average bands at site 000. The χ^2 misfit is acceptable at all periods. Comparing Figs. 6 and 7 reveals that the electric field distortion parameters are now smoother and less period dependent. The magnetic distortion parameters (not shown) are also relatively constant with period. This shows that electric-only distortion is an inadequate description at periods shorter than 40 s, suggesting that inclusion of magnetic field galvanic distortion is appropriate for the Nelson batholith sites. Increasing the width of the bands over which the parameters are fit yields the expected smoother parameter behaviour, but also results in unacceptable misfit at periods shorter than 10 s.

Based on the observed behaviour of the frequency-dependent distortion model fits, frequency-independent models were fit separately to the site 000 data at periods shorter and longer than 10 s. The model fit is acceptable at the 95% level for the longer period band, but χ^2 is 20–70 at the short period end. The resulting twist, shear, and azimuth values at periods longer than 10 s

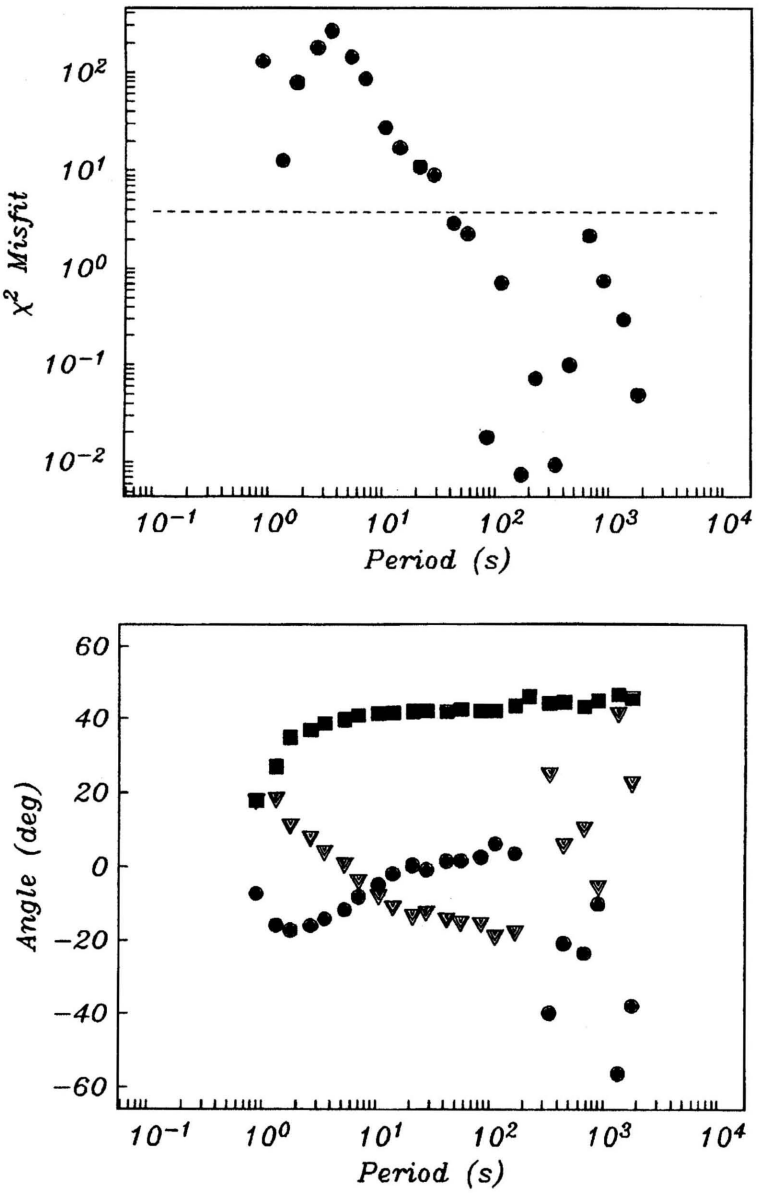

Fig. 6. The χ^2 misfit (top panel) and electric field distortion parameters (bottom panel) plotted against period for a frequency-by-frequency electric field galvanic distortion decomposition of the MT response at site 000. The dashed horizontal line in the top panel denotes the 95% critical value for 1 degree of freedom. The three quantities shown in the bottom panel are twist (circles), shear (squares), and regional azimuth (triangles).

are 2.1°, 42.0°, and −14.9°, respectively, and are changed only slightly below 10 s. The magnetic distortion parameters γ and ε are 0.018 and −0.00084 at periods longer than 10 s. A frequency-independent electric-only distortion decomposition can be fit acceptably only at periods longer than 50 s and gives essentially the same distortion parameters over that range. These results indicate that magnetic field galvanic distortion is present in the site 000 data, but the inability to get an acceptable statistical fit at periods under 10 s further suggests that inductive phenomena

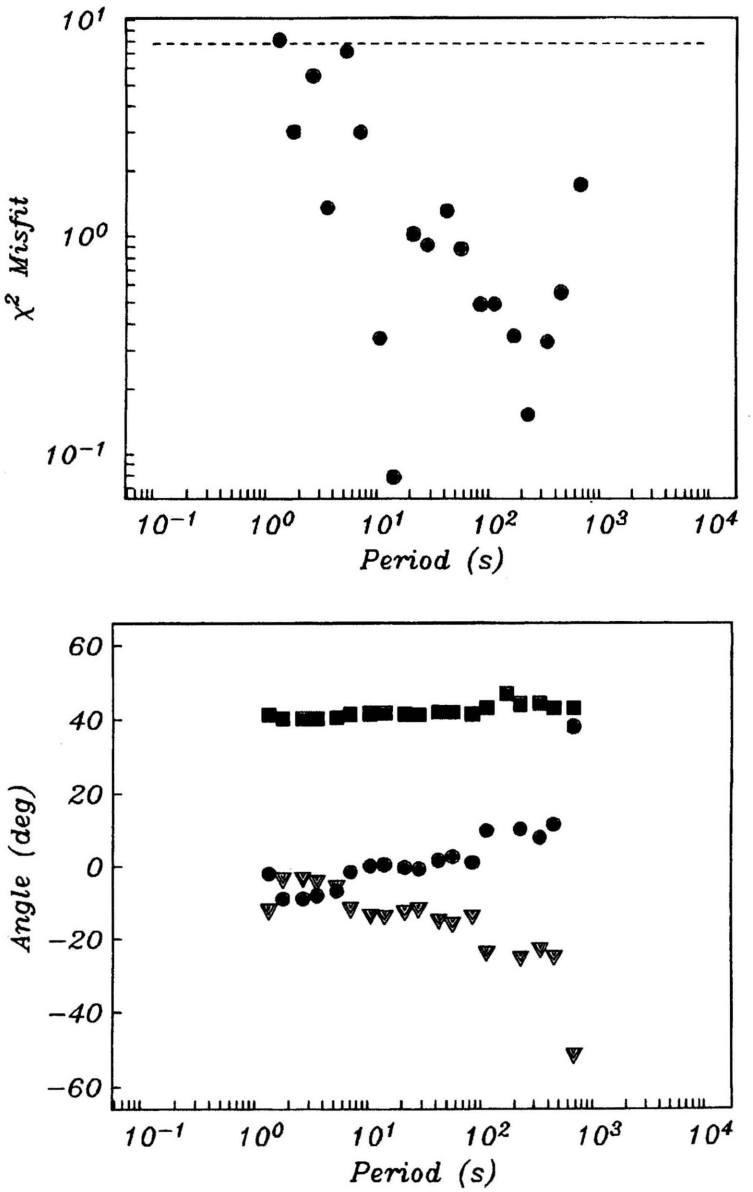

Fig. 7. The χ^2 misfit (top panel) and electric field distortion parameters (bottom panel) plotted against period for an electric and magnetic field galvanic distortion decomposition of the MT response at site 000 computed over running average bands 3 frequencies wide. The dashed horizontal line in the top panel denotes the 95% critical value for 3 degrees of freedom. The three quantities shown in the bottom panel are twist (circles), shear (squares), and regional azimuth (triangles).

also influence the data.

However, the resulting principal apparent resistivities and phases are not consistent with a 2D structure (Fig. 8); the phase of the b direction ($\theta = 75.1°$) is in excess of 90° and hence out-of-quadrant. Similar analysis on site 004 yields comparable frequency-independent distortion parameters to those at site 000. The principle apparent resistivities and phases are different

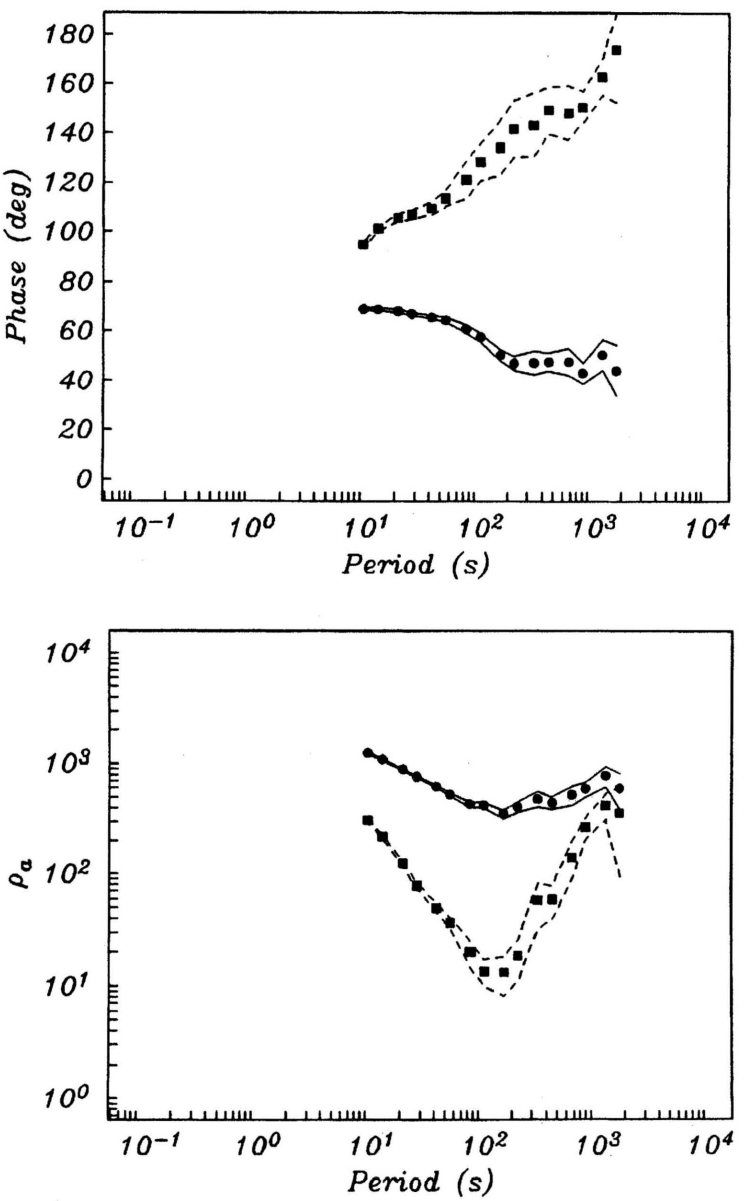

Fig. 8. The phase (top panel) and apparent resistivity (bottom panel) for a frequency-independent fit of an electric and magnetic field galvanic distortion model to the site 000 data at periods longer than 10 s. The symbols denote the estimates, while the solid and dashed lines show the double-sided 95% confidence bands. The circles and solid lines correspond to the a direction ($\theta = -14.9°$) while the squares and dashed lines correspond to the b direction ($\theta = 75.1°$). Angles are defined clockwise from true north.

in form, but the out-of-quadrant phase for the b direction is still present, although it is nearly frequency-independent at periods under 300 s with a value near 100°. Thus, the best-fitting response obtained from the electric and magnetic distortion decomposition is that of an anti-diagonal 3D structure. Note that Eqs. (1)–(5) only state that the regional structure is anti-diagonal in form, and no further requirement of a 2D structure is implied. Similar out-of-quadrant

phases were observed by Jones *et al.* (1993) for all sites located on the batholith. Given the complex geometry of the Nelson batholith, this is perhaps not too surprising. It must be concluded that either 3D non-galvanic effects are dominant, or that the tensor decomposition model is not applicable, or that the minimum solutions found are not necessarily the best ones for a physical description of the regional responses. As emphasized in the remarks on decomposition (Section 2), the solution is sought which tries to minimize a complex set of parameters to the model. Most of the time this has the effect of minimizing the diagonal components, thus attempting to make the description of the regional response anti-diagonal; no other physical constraints are applied. The solution found may be the one that yields the minimum misfit, but, given the error distribution, there may exist other acceptable solutions which yield a 2D regional response but which do not necessarily lead to a minimum misfit. For these data, rotation of the impedance tensor shows that it is possible to find a strike angle that constrains the two phases to lie in the first quadrant, and that angle is between 31°–61° for periods up to 250 s.

5.3 Off-Nelson batholith response (Site 006)

Site 006 is located east of the Nelson batholith and near the boundary between a volcanic province and a slice of the Purcell continental margin sediments (Fig. 1). The raw MT response tensor is qualitatively similar in morphology and magnitude to the Nelson batholith response at site 004. Figure 9 shows the χ^2 misfit and electric distortion parameters for an electric-only tensor decomposition of these data. The misfit is unacceptable under a 95% criterion at periods shorter than 100 s, and rises rapidly as period decreases below that point. The distortion parameters are increasingly frequency-dependent as period decreases. Attempts to force a frequency-independent fit for periods longer than 20 s, where the parameters are relatively constant, fails; the misfit remains large at periods under 10 s. Figure 10 shows the fit of a frequency-independent model to the data; in particular the $Re(Z_{xx})$ and $Im(Z_{xy})$ are badly fit.

However, inclusion of magnetic field galvanic distortion in the model leads to an acceptable fit at periods longer than 10 s. The resulting electric distortion parameters are very similar to those in Fig. 9 except that the azimuth shows more scatter, and the magnetic field distortion parameters are quite frequency-independent. It is possible to fit a frequency-independent electric and magnetic field distortion model for periods longer than 20 s. The resulting twist, shear, and azimuth are 21.3°, 9.8°, and −37.9°, respectively, while the magnetic distortion parameters γ and ε are 0.025 and −0.023. Figure 11 shows the principal apparent resistivities and phases from the decomposition. The b component at an azimuth of 52° is poorly determined at periods over 1000 s so that its phase is practically meaningless, reflecting the much smaller magnitude of the response in that direction. However, the phase does remain in quadrant and the MT response is interpretable in a 2D sense, unlike the Nelson batholith responses at sites 000 and 004, which are certainly close in an inductive sense at periods in excess of 100 s.

5.4 Kootenay Arc response (Sites 009 and 007)

Sites 009 and 007 are located on upper Proterozoic to lower Cambrian continental margin sediments, and both display strongly E-W polarized electric fields such that the Z_{yx} and Z_{yy} components are 5–10 times larger than the Z_{xx} and Z_{xy} components. Note also that sites 007 and 008 were collected as a ten channel pair, but the site 008 response is markedly different than that at site 007 (Jones and Groom, 1993).

A frequency-by-frequency electric-only decomposition of the site 007 data yields an acceptable fit at periods longer than 10 s, and increasing misfit at shorter periods. However, the resulting twist and regional azimuth are widely scattered, although the shear remains relatively constant across period. Inclusion of magnetic distortion improves the fit only slightly. Site 009 shows very similar characteristics except that the electric distortion fit is less acceptable, and the addition of

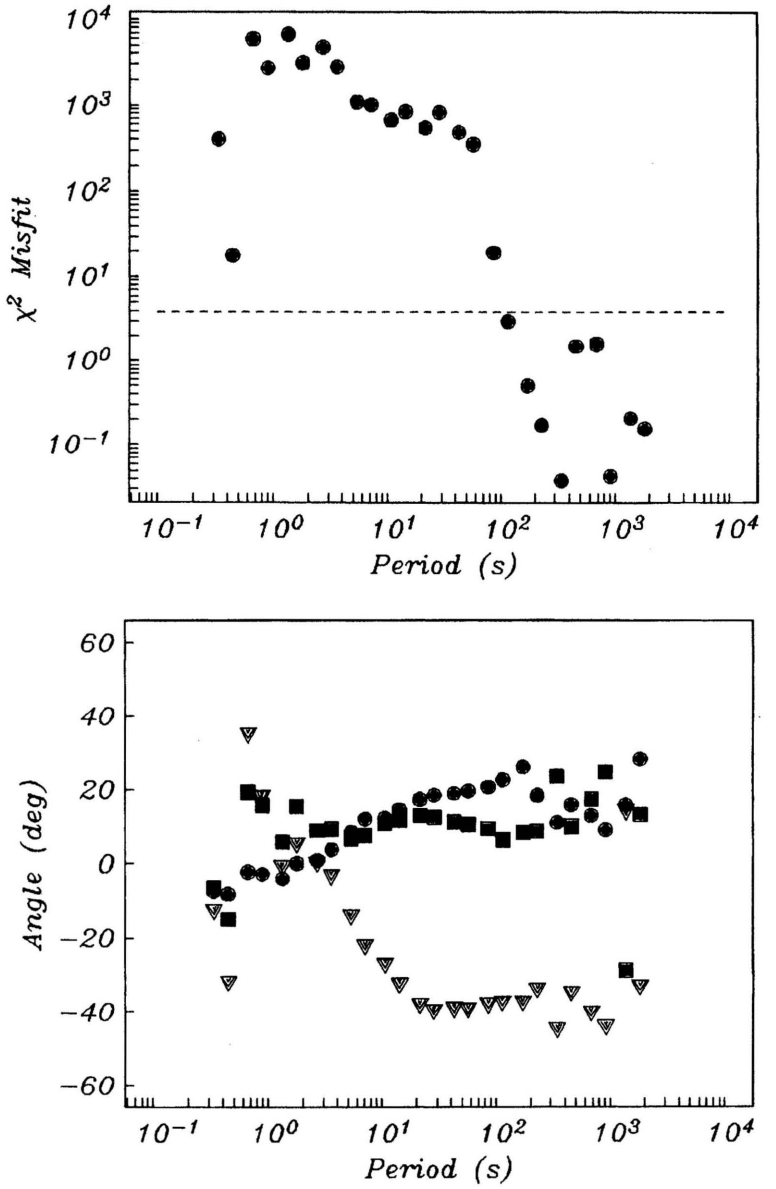

Fig. 9. The χ^2 misfit (top panel) and electric field distortion parameters (bottom panel) plotted against period for a frequency-by-frequency electric field galvanic distortion decomposition of the MT response at site 006. The dashed horizontal line in the top panel denotes the 95% critical value for 1 degree of freedom. The three quantities shown in the bottom panel are twist (circles), shear (squares), and regional azimuth (triangles).

magnetic field distortion results in overfitting at periods longer than 10 s, with χ^2 values always under 2 using 3-frequency-wide running average bands.

A frequency-independent electric field only distortion model can be fit under a 95% criterion to the site 007 data for periods longer than 10 s. The twist, shear, and regional azimuth are, respectively, 38.3°, −43.0°, and −66.0°. The twist and shear approach 45°, indicating very strong surface galvanic distortion; this is the singular decomposition regime of Groom *et al.* (1993) and

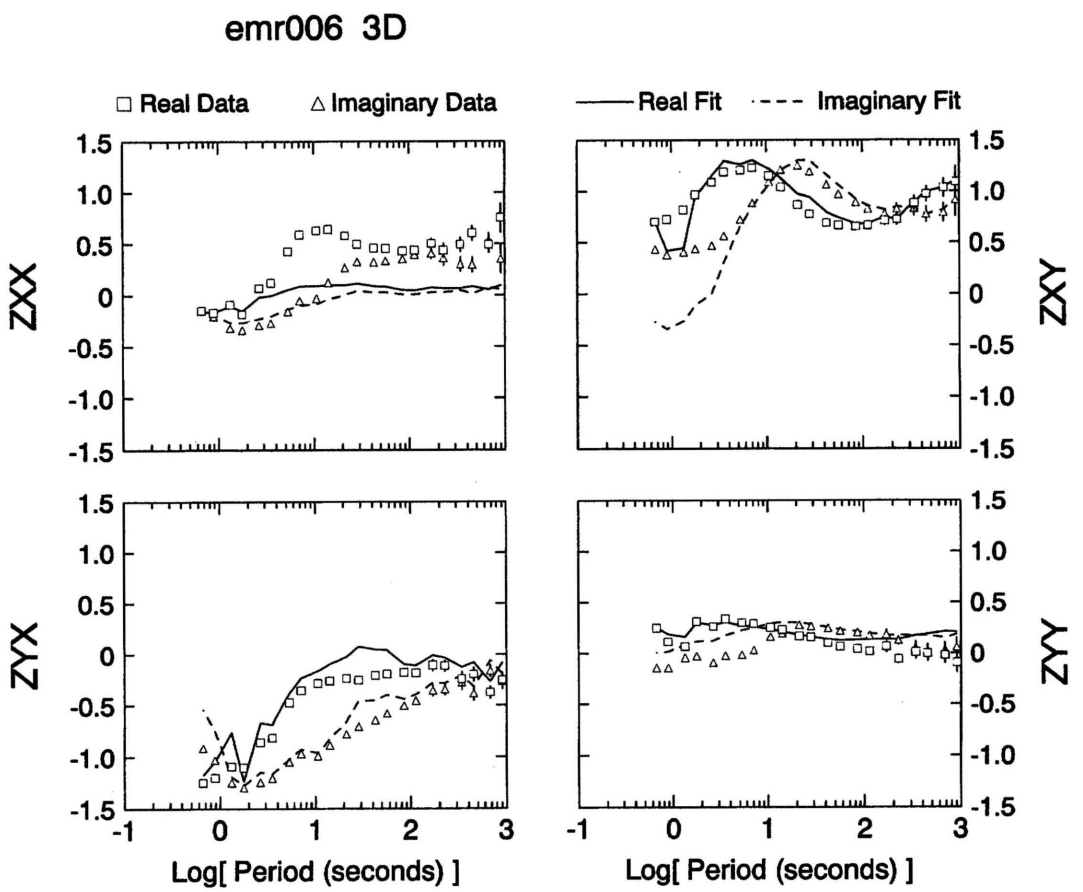

Fig. 10. The fit of the frequency-independent electric field only decomposition model to the data from site 006. The response functions are shown as symbols with 95% error bars, with squares and triangles denoting the real and imaginary parts, respectively. The model responses are shown as solid and dashed lines for the real and imaginary parts, respectively.

Jones *et al.* (1993) in which current channeling is so severe that they were unable to extract both principal responses in the presence of noise. This is not the case for either site 007 or 009, reflecting the smaller errors in these data compared to the Phoenix-processed ones. Figure 12 shows the resulting principal apparent resistivities and phases at site 007. The b direction at an azimuth of 24° is poorly determined only at periods longer than 500 s, reflecting the weak electric field and small apparent resistivity, but the corresponding phase is out-of-quadrant at periods longer than 200 s. The addition of magnetic field distortion to the model improves the fit only slightly, but does reduce the size of the twist considerably and flattens the b phase, bringing it into the first quadrant out to periods of 400 s. In contrast, at site 009 a frequency-independent electric field model fit for periods longer than 10 s is inadequate below 100 s, while the inclusion of magnetic field distortion yields a good fit at all periods. Unlike site 007, the resulting decomposed response is 2D, but the b phase is poorly determined beyond 500 s.

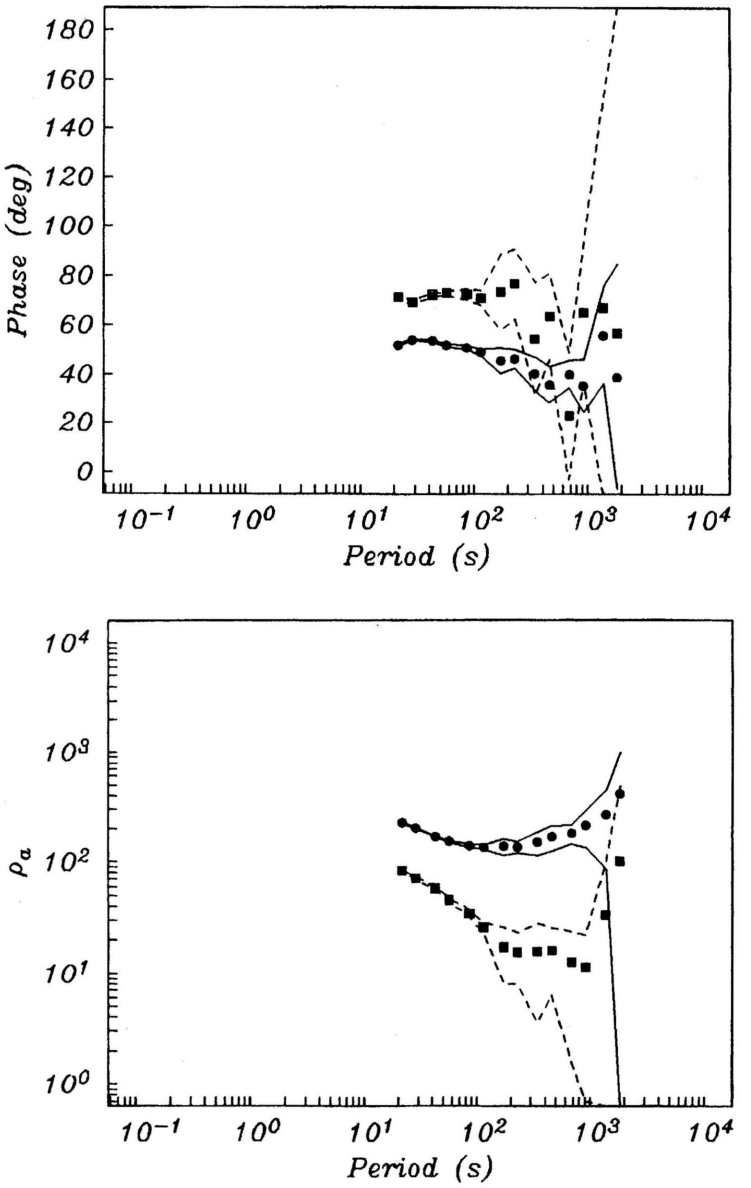

Fig. 11. The phase (top panel) and apparent resistivity (bottom panel) for a frequency-independent fit of an electric and magnetic field galvanic distortion model to the site 006 data at periods longer than 20 s. The symbols denote the estimates, while the solid and dashed lines show the double-sided 95% confidence bands. The circles and solid lines correspond to the a direction ($\theta = -37.9°$) while the squares and dashed lines correspond to the b direction ($\theta = 52.1°$). Angles are defined clockwise from true north.

5.5 Purcell sediment response (Sites 008, 016, and 019)

The remaining three sites are located on the Purcell continental margin sediments east of the Kootenay arc (Fig. 1). Neither an electric nor an electric plus magnetic field tensor decomposition fits any of them completely, probably reflecting regional 3D effects.

At site 008, which is located closest to the Kootenay Arc, a frequency-by-frequency electric

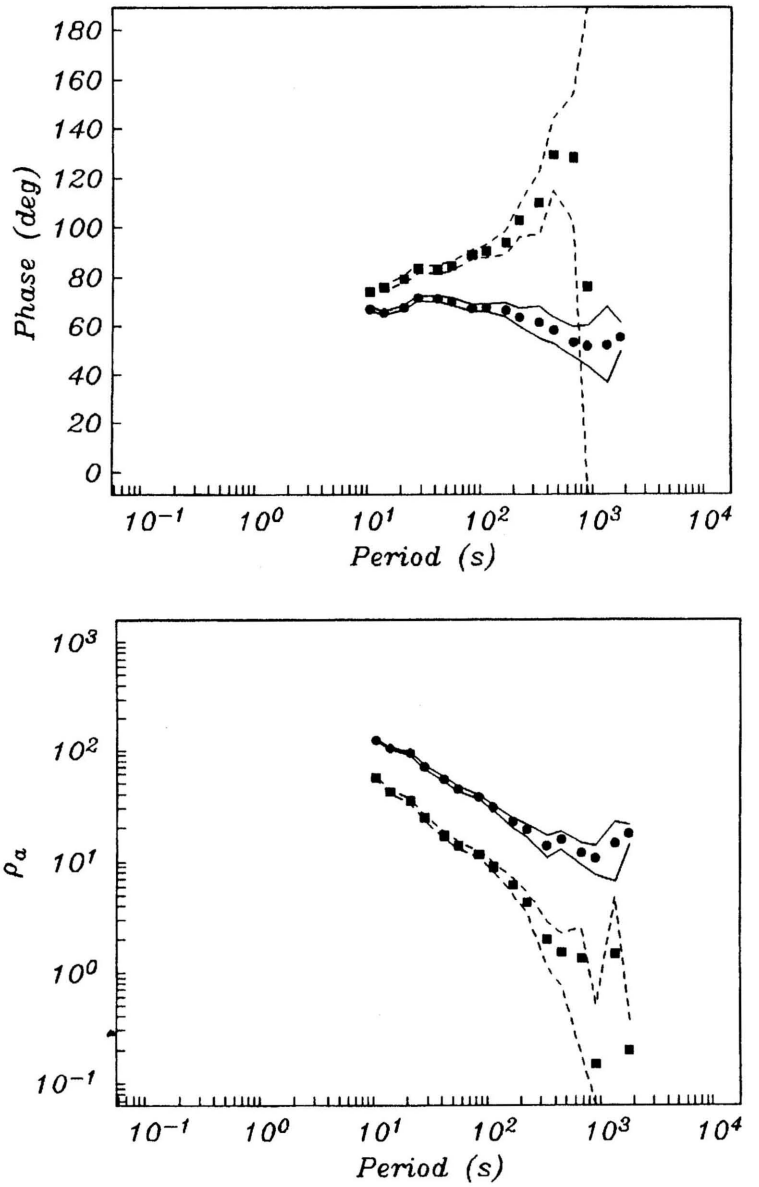

Fig. 12. The phase (top panel) and apparent resistivity (bottom panel) for a frequency-independent fit of an electric field galvanic distortion model to the site 007 data at periods longer than 10 s. The symbols denote the estimates, while the solid and dashed lines show the double-sided 95% confidence bands. The circles and solid lines correspond to the a direction ($\theta = -66.0°$) while the squares and dashed lines correspond to the b direction ($\theta = 24.0°$). Angles are defined clockwise from true north.

field distortion model does not fit the data adequately, displaying excess misfit at the 95% level that is widely spread across the period range. However, the addition of magnetic field galvanic distortion does yield an adequate fit at all save the shortest and longest periods and a relatively smooth set of electric field distortion parameters (Fig. 13). The twist and shear undergo a large step-like change at about 50 s period, with the suggestion of a smaller shift in the azimuth at

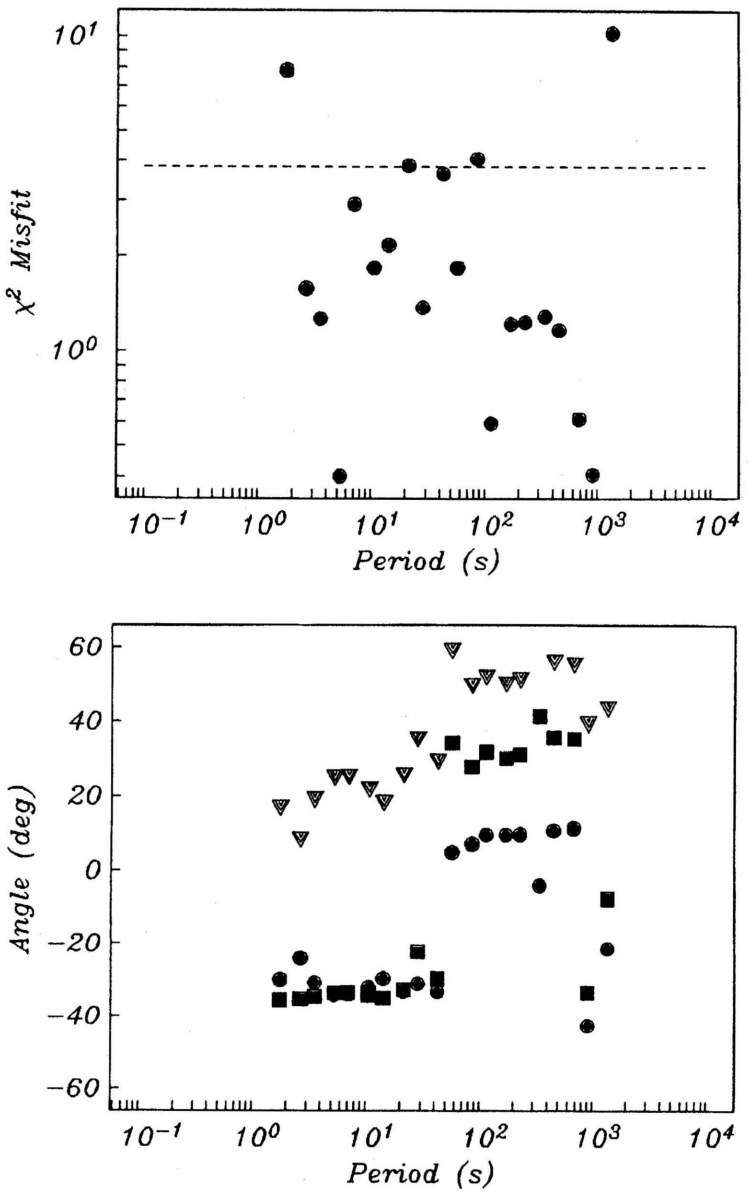

Fig. 13. The χ^2 misfit (top panel) and electric field distortion parameters (bottom panel) plotted against period for an electric and magnetic field galvanic distortion decomposition of the MT response at site 008 computed over running average bands 3 frequencies wide. The dashed horizontal line in the top panel denotes the 95% critical value for 3 degrees of freedom. The three quantities shown in the bottom panel are twist (circles), shear (squares), and regional azimuth (triangles).

the same point. The magnetic distortion parameters also undergo a step-like decrease at about the same point. This is not seen at either site 016 or 019, and in fact neither of those datasets is adequately fit by a frequency-by-frequency electric and magnetic distortion model, although the resulting distortion parameters are smooth functions of period. Finally, it is possible to fit the site 008 data with a frequency-independent electric and magnetic field (but not electric field

only) distortion model at periods longer than 50 s; the resulting principal responses are 2D in form. It is not possible to fit a frequency-independent model of either type at sites 016 or 019.

6. Conclusions

Models of the Earth based on MT data are, at best, only as good as the quality of the regional responses derived, and are functionally dependent on knowing the class of the underlying regional structure (e.g., 2D versus 3D) gleaned from the raw impedance tensor estimates. We have shown that superior estimates, particularly of errors, can be determined from MT data, and that careful study of these data for distortion effects can indicate period bands appropriate for adopting an electric-only distortion model, or an electric and magnetic field distortion model.

The re-processed data from the BC87 sites show that local 3D distortion of a 2D regional conductivity structure is a poor universal description of the responses, but does serve well for some sites over fairly broad period bands. The failure of that model probably results from a breakdown of the basic assumptions that control its validity. In particular, for all sites on the Nelson batholith there is a change in regime at around the period of the inductive scale size of the body, or around 3–5 s for the 50 by 150 km body of 15,000 Ωm resistivity. It is unlikely that the background electric field will be uniform over such a large 3D body embedded in a regional 2D earth. The inadequacy of a distortion model to describe the large-scale batholith effects is most apparent by comparing the on-batholith responses (000 and 004) with the off-batholith one (006). At sufficiently long periods the responses should be the same, and they are decidedly not. In addition, as noted by Jones (1993), early studies suggest that the regional conductivity structure is 3D rather than 2D.

An important use of, and advantage from, applying decomposition methodology to the data is that one obtains a guide to suggest the level of misfit when modelling the regional responses by a 2D code. If the decomposition model only fits the data to a χ^2 of say 100, and the typical phase error is 1°, then the decomposition model is fitting the data to 4–5° on average. Accordingly, there is little sense fitting a 2D model to any smaller level of misfit, as one is then probably fitting artifacts of the 2D parameterization of the 3D real Earth, rather than real 2D structure.

One note of caution that this study reinforces is that clearly one should not routinely apply decomposition analysis without thought. Care must be taken to assess the fit not only in statistical terms but also visually (e.g., Figs. 4 and 8) to ensure that all significant features of the data are described by the model.

The BC87 data were acquired by Phoenix Geophysics Ltd.; Gerry Graham and George Elliot ensured as high a data quality as possible. This work was supported at WHOI by the Office of Basic Energy Sciences, US Department of Energy. This is Woods Hole Oceanographic Institution contribution 9165, Geological Survey of Canada contribution number 28195, and Lithoprobe publication number 730.

REFERENCES

Bahr, K., Elimination of local 3D distortion of the magnetotelluric tensor impedance allowing for two different phases, Contributed paper at "Seventh Workshop on Electromagnetic Induction in the Earth and Moon", held in Ile-Ife, Nigeria, on August 15–22, 1984.

Bahr, K., Magnetotellurische messung des elektrischen widerstandes der erdkruste und des oberen mantels in gebieten mit lokalen und regionalen leitfähigkeitsanomalien, Ph.D. thesis, Univ. Göttingen, 1985 (in German).

Bahr, K., Interpretation of the magnetotelluric impedance tensor: regional induction and local telluric distortion, *J. Geophys.*, **62**, 119–127, 1988.

Berdichevsky, M. N. and V. I. Dmitriev, Distortion of magnetic and electric fields by near-surface lateral inhomogeneities, *Acta Geodaet., Geophys. et Montanist. Acad. Sci. Hung.*, **11**, 447–483, 1976a.

Berdichevsky, M. N. and V. I. Dmitriev, Basic principles of interpretation of magnetotelluric sounding curves, in *Geoelectric and Geothermal Studies*, edited by A. Ádám, KAPG Geophysical Monograph, Akadémiai Kiadó, 165–221, 1976b.

Boerner, D. E., R. D. Kurtz, J. A. Craven, S. Rondenay, and W. Qian, A buried Proterozoic foredeep under the Western Canada sedimentary basin?, *Geology*, **23**, 297–300, 1995.

Chakridi, R., M. Chouteau, and M. Mareschal, A simple technique for analysing and partly removing galvanic distortion from the magnetotelluric impedance tensor: application to Abitibi and Kapuskasing data (Canada), *Geophys. J. Int.*, **108**, 917–929, 1992.

Chave, A. D. and D. J. Thomson, Some comments on magnetotelluric response function estimation, *J. Geophys. Res.*, **94**, 14,215–14,225, 1989.

Chave, A. D. and D. J. Thomson, Robust, controlled leverage estimation of magnetotelluric response functions, Contributed paper at "11th Workshop on Electromagnetic Induction", held in Wellington, New Zealand, on 26 August–2 September, 1992.

Chave, A. D. and J. T. Smith, On electric and magnetic galvanic distortion tensor decompositions, *J. Geophys. Res.*, **99**, 4669–4682, 1994.

Eisel, M. and K. Bahr, Electrical anisotropy in the lower crust of British Columbia: an interpretation of a magnetotelluric profile after tensor decomposition, *J. Geomag. Geoelectr.*, **45**, 1115–1126, 1993.

Groom, R. W., The effects of inhomogeneities on magnetotellurics, Ph.D. Thesis, Univ. Toronto, 212 pp., 1988.

Groom, R. W. and R. C. Bailey, Decomposition of magnetotelluric impedance tensors in the presence of local three-dimensional galvanic distortion, *J. Geophys. Res.*, **94**, 1913–1925, 1989.

Groom, R. W. and K. Bahr, Corrections for near surface effects: decomposition of the magnetotelluric impedance tensor and scaling corrections for regional resistivities: a tutorial, *Surv. Geophys.*, **13**, 341–380, 1992.

Groom, R. W., R. D. Kurtz, A. G. Jones, and D. E. Boerner, A quantitative methodology for determining the dimensionality of conductive structure from magnetotelluric data, *Geophys. J. Int.*, **115**, 1095–1118, 1993.

Gupta, J. C. and A. G. Jones, Electrical conductivity structure of the Purcell Anticlinorium in southeast British Columbia and northwest Montana, *Can. J. Earth Sci.*, **32**, 1564–1583, 1995.

Jones, A. G., The BC87 dataset: tectonic setting, previous EM results, and recorded MT data, *J. Geomag. Geoelectr.*, **45**, 1089–1105, 1993.

Jones, A. G. and I. Dumas, Electromagnetic images of a volcanic zone, *Phys. Earth Planet. Int.*, **81**, 289–314, 1993.

Jones, A. G. and R. W. Groom, Strike angle determination from the magnetotelluric tensor in the presence of noise and local distortion: rotate at your peril!, *Geophys. J. Int.*, **113**, 524–534, 1993.

Jones, A. G., R. D. Kurtz, D. W. Oldenburg, D. E. Boerner, and R. Ellis, Magnetotelluric observations along the LITHOPROBE southeastern Canadian Cordilleran transect, *Geophys. Res. Lett.*, **15**, 677–680, 1988.

Jones, A. G., A. D. Chave, G. Egbert, D. Auld, and K. Bahr, A comparison of techniques for magnetotelluric response function estimation, *J. Geophys. Res.*, **94**, 14,201–14,213, 1989.

Jones, A. G., R. W. Groom, and R. D. Kurtz, Decomposition and modelling of the BC87 dataset, *J. Geomag. Geoelectr.*, **45**, 1127–1150, 1993.

Kurtz, R. D., J. A. Craven, E. R. Niblett, and R. A. Stevens, The conductivity of the crust and mantle beneath the Kapuskasing Uplift: electrical anisotropy in the upper mantle, *Geophys. J. Int.*, **113**, 483–498, 1993.

Larsen, J. C., Low frequency (0.1–6.0 cpd) electromagnetic study of deep mantle electrical conductivity beneath the Hawaiian islands, *Geophys. J. Royal Astron. Soc.*, **43**, 17–46, 1975.

Larsen, J. C., Removal of local surface conductivity effects from low frequency mantle response curves, *Acta Geodaet., Geophys. et Montanist. Acad. Sci. Hung.*, **12**, 183–186, 1977.

Marquis, G., A. G. Jones, and R. D. Hyndman, Coincident conductive and reflective lower crust across a thermal boundary in southern British Columbia, Canada, *Geophys. J. Int.*, **120**, 111–131, 1995.

Ogawa, Y., Y. Nishida, and M. Makino, A collision boundary imaged by magnetotellurics, Hidaka Mountains, central Hokkaido, Japan, *J. Geophys. Res.*, **99**, 22,373–22,388, 1994.

Smith, J. T., Understanding telluric distortion matrices, *Geophys. J. Int.*, **122**, 219–226, 1995.

Thomson, D. J. and A. D. Chave, Jackknifed error estimates for spectra, coherences, and transfer functions, in *Advances in Spectrum Analysis and Array Processing, Vol. 1*, edited by S. Haykin, pp. 58–113, Prentice-Hall, Englewood Cliffs, NJ, 1991.

Vozoff, K., (ed.), *Magnetotelluric Methods*, Soc. Expl. Geophys. Reprint Ser. No. 5, Publ. by Soc. Expl. Geophys., Tulsa, Oklahoma, ISBN 0-931830-36-2, 1986.

Wight, D. E. and F. X. Bostick, Cascade decimation—a technique for real time estimation of power spectra, Contributed paper at "*Proc. IEEE Intl. Conf. on Acoust., Speech, Signal Proc.*, 626–629", held in Denver, CO, on April 9–11, 1980, Reprinted in Vozoff, 1986.

Zhang, P., R. G. Roberts, and L. B. Pedersen, Magnetotelluric strike rules, *Geophys.*, **52**, 267–278, 1987.